ISSN 0915-633X

NATIONAL INSTITUTE FOR FUSION SCIENCE

Configuration Studies of LHD Plasmas

M. Okamoto

(Received - Feb. 25, 1997)

NIFS-487 Mar. 1997

RESEARCH REPORT
NIFS Series

NAGOYA, JAPAN

Configuration Studies of LHD Plasmas*

Masao Okamoto
National Institute for Fusion Science, Nagoya 464-01, Japan

Abstract

Configuration studies are performed on the plasmas of The Large Helical Device (LHD), the construction of which is almost completed at the National Institute for Fusion Science. The LHD has flexibility as an experimental device and can have various configurations by changing the poloidal magnetic fields, the pitch of the helical coils (pitch parameter), and the ratio of currents flowing in the two helical coils. Characteristics of the plasma are investigated for the standard configuration, the change in the pitch parameter, and the helical axis configuration.

Keywords: helical system, LHD, CHS, configuration study, interchange mode, Mercier criterion, bootstrap current, radial electric field

---

* Presented at the JIFT workshop on "Advanced Fusion Concept and theory" held at Columbia University. October 14 to 17. 1996.

1. Introduction

Helical systems or stellarators are of great advantage to a steady state operation without power for current drive, because they can be operated in the currentless mode. Another advantage is that the helical systems are free from plasma disruptions which are serious in tokamaks. The success in realizing currentless plasmas in W7-A[1] and Heliotron-E[2] has demonstrated that the helical systems are promising fusion devices comparable to tokamaks. Heliotron-E is a planar axis helical system with $L = 2$ and $M = 19$, where L and M are poloidal and toroidal helical polarities. It has a large aspect ratio, $A = R/\bar{a}_p \simeq 11$ (R is the major radius and $\bar{a}_p$ is the average plasma radius) and the large magnetic shear. Subsequently to the successful experimental results on Heliotron-E [2], ATF was designed to increase the beta limit by lowering the aspect ratio ($A \simeq 7$)[3]. To improve further the MHD stability, three pairs of axisymmetric poloidal coils are equipped in ATF, which can control the rotational transform and the magnetic well region[4]. CHS has been designed to investigate currentless plasmas in a compact heliotron with the aspect ratio ($A \simeq 5$)[5]. Recently, the average beta value of 2.1% was achieved in CHS, which is the world record in helical systems[6]. Based on the fruitful results from Heliotron-E, ATF, and CHS, a large heliotron-type device called the Large Helical Device (LHD) was designed [7] and the construction has been started in 1989 at The National Institute for Fusion Science (NIFS).

The purpose of The Large Helical Device (LHD), which is a helical system of the heliotron configuration, is to perform physics experiments extrapolatable to fusion conditions by producing a currentless plasma with a divertor configuration. The LHD aims at achieving long pulse or steady state operations with superconducting magnetic coils. Experimental and theoretical understanding of confinement physics common to toroidal plasmas such as in helical systems and tokamaks is also a purpose. The basic machine parameters for LHD are as follows [7] : poloidal and toroidal helical polarities are $L = 2$ and $M = 10$, respectively, the major radius is $R_0 = 3.9$m, the maximum magnetic field is $B_0 = 3T$. The LHD coil system consists of two helical coils and three pairs of axisymmetric poloidal coils. All the coils are super conductors. The two helical coils are wound on the surface of the torus, the poloidal cross section of which is a circle around the point $(R_0 = 3.9m, Z_0 = 0)$. The winding law of the helical coils is $\theta = M\phi/L + \alpha \sin(M\phi/L)$ with the

pitch modulation $\alpha = 0.1$, where θ and ϕ are the poloidal and toroidal angle, respectively.

MHD equilibrium and stability, particle orbits, ripple diffusion, bootstrap current, and many other physics processes depend strongly on the magnetic field structure or configuration. Generally, helical systems are flexible as an experimental device in a sense that they can be externally controlled to make various configurations. Theoretical studies of physics phenomena on the configuration are extensively reviewed on the helical systems with a planar circular axis[8]. The LHD has remarkable freedoms or flexibility as an experimental device. One of them is that the two helical coils have a multi-layer structure for flowing coil currents. The current can be flowed independently in each current layer. The coil radius a_c is defined as the minor radius length from the coil center ($R_0 = 3.9m$, $Z_0 = 0$) to the center of the currents flowing in the helical coil. The pitch of the helical coils (pitch parameter) is given by $\gamma_c = Ma_c/(LR_0)$. It has shown that this parameter should be $\gamma_c \simeq 1.2 \sim 1.5$ to obtain a substantial plasma volume[9]. Each helical coil has three current layers and the coil radius a_c can be changed by the combination of three layers in which a current is flowed. The pitch parameter is $\gamma_c = 1.25$ for full operation (currents are flowed in all layers). The changeable a_c or γ_c is one of experimental freedoms, because the pitch parameter γ_c affects the formation of magnetic well/hill and shear and thus MHD properties. The coil current in one helical coil (say, I_{h1}) and the current in another helical coil (say, I_{h2}) are the same ($I_{h1} = I_{h2}$) under the normal operation. However, the two helical coils are independent and not linked. It is possible to change the ratio of I_{h1}/I_{h2} ($I_{h1} \neq I_{h2}$) to produce Fourier components of the magnetic field strength with $l = 1$ and $m = 5$. Three pairs of axisymmetric poloidal coils are equipped in the LHD coil system. The poloidal fields can control the plasma position by changing the dipole component, the ellipiticity of the plasma cross section by changing the quadruple component, and the flux swing or flux leakage.

We can thus obtain various configurations for the LHD changing the poloidal fields, the ratio I_{h1}/I_{h2}, and the pitch parameter γ_c of the two helical coils. The configuration with $B = 3T$, $\gamma_c = 1.25$, and $I_{h1} = I_{h2}$ is optimized by changing poloidal fields so as to satisfy three physics conditions; (a) achievement of high plasma beta value of 5%, (b) good confinement of energetic particles, and (c) effective built-in divertor configuration. This configuration is called the "standard configuration". Controlling the poloidal

fields, we can realize the standard configuration, in which the plasma position is inwardly shifted by 0.15m in vacuum from the coil center ($R_0 = 3.9$m, $Z = 0$) and the plasma cross-sections are nearly circular if toroidally averaged. Experiments on LHD will be carried out changing the configuration in the parameter space around the standard configuration. However, the configuration has not been optimized taking into account minimization of the bootstrap current. In planar axis helical systems, it is difficult to obtain a configuration satisfying simultaneously the high plasma beta, good particle orbits (or reduced ripple diffusion), and the minimum bootstrap current.

In section 2, we consider the control and optimization of poloidal fields to obtain the standard configuration. We investigate MHD properties (stabilities against the Mercier or interchange mode, kink mode, and ballooning mode), particle orbit, ripple diffusion, and bootstrap current. In section 3, we examine the effect of change in the pitch parameter γ_c on the MHD characteristics. In section 4, the configuration with unbalanced helical coil currents ($I_{h1} \neq I_{h2}$) is considered with emphasis on the change in bootstrap currents. Summary is given in section 5.

2. Control of Poloidal Fields and the Standard Configuration

2.1 Optimization

The LHD has three pairs of axisymmetric poloidal coils. Adjusting a current in each poloidal coil, we can change the dipole and quadruple components denoted here by B_v and B_q, respectively, to control the plasma position and the ellipticity of plasma cross-sections. This flexibility was claimed as one of the main advantages of ATF[4] and employed in LHD.

In LHD, the magnetic axis of the vacuum field can be shifted by 0.3m from the coil center ($R_0 = 3.9m, Z_0 = 0$) by controlling the dipole field B_v. As the plasma is shifted inward, the magnetic well area becomes small to worsen the stability of Mercier mode or interchange mode. On the other hand, the orbit confinement of a single particle is remarkably improved as the plasma is shifted inward, and hence the ripple diffusion is significantly reduced. A compromise should be reached between the two. The criteria for the compromise are ; (a) to obtain a high beta plasma with $< \beta > \simeq 5\%$, (b) to obtain a good confinement of energetic particles with no loss cone in the region within one-third of the plasma minor radius. and (c) to obtain a natural build-in

divertor configuration in which there is enough clearance between the plasma boundary and the first wall. (In CHS, the plasma touches the first wall if it is shifted inward.) The ellipticity can be added to the plasma cross-section by controlling B_q to elongate the plasma cross-section in the horizontal or vertical direction. This shaping of the plasma cross-section (B_q-control) affects the confinement of energetic particles and MHD stabilities, although it is less effective than the plasma positioning (B_v-control). The remarkable effect of plasma shaping is to alter the magnitude of the bootstrap current significantly. However, it should be noted that the dependencies of the ripple diffusion (or particle orbit) and the bootstrap current on the configuration are different and that the compromise between the two is difficult in planar axis helical systems.

For the currentless plasma, the most important MHD modes are pressure-driven modes. The Mercier criterion has been investigated in Ref. [10] for the LHD plasma changing the plasma position and the plasma beta value. The VMEC code [11] was used to calculate LHD equilibria with the peaked pressure profile of $P = P_0(1-\Phi_n)^2$, where Φ_n is the normalized toroidal flux. Fiure 1 shows the stability diagram of Mercier criterion and the equilibrium beta limit. The Mercier criterion D_M given by Glasser, Green, and Johnson[12] is calculated and contours of $D_I = -D_M/(\iota')^2$ are plotted in Fig.1, where ι' is the derivative of the rotational transform ι. By Δ_v, we denote the shift of the magnetic axis in the vacuum fileld from the position $R_0 = 3.9$m ($\Delta_v = 0$ corresponds to $R_0 = 3.9$m). The solid line marked by $D_I = 0$ is the Mercier criterion and the dotted lines are contours of level surfaces with increment of $\Delta D_I = 0.1$. The plasma is slightly Mercier unstable for $\Delta_v = -0.15$m. Numerical studies for stability of low$-n$ ideal interchange modes with the KSTEP code based on the stellarator expansion [13] and the fully three dimensional TERPSICHORE code [14] have shown that the low$-n$ modes may be marginally unstable with very small growth rate near the Mercier boundary. However, such marginally unstable modes can easily be stabilized by some kinetic effects such as the finite Larmor effect. Thus the plasma with $\Delta_v = -0.15$m can be actually stable against the low$-n$ ideal interchange modes. If the magnetic axis is shifted in the outward direction of the major radius, the plasma becomes more stable against the interchange modes and completely stable if $\Delta_v \geq -0.1$m. On the other hand, the plasma becomes unstable with inward shift. If $\Delta_v = -0.2$m, some low$-n$ interchange modes are unstable. However, the second stability regime persists in

the region above $\beta_0 \sim 6\%$, where β_0 is the plasma beta value at the plasma center. It is estimated that the hatched region in Fig.1 is unstable against low-n ideal interchange modes. It is noted that access to the second stability regime has been achieved in ATF[15]. The equilibrium beta limit gradually increases with the inward shift of the plasma position. However, the variation of the equilibrium beta limit with the inward shift is small and the calculation results show that the average equilibrium beta limit is larger than or equal to 5%. In the case of a peaked pressure profile like $P = P_0(1 - \Phi_n)^2$, the Shafranov shift is large as the beta increases extending the magnetic well region to stabilize the interchange mode. However, if the pressure profile is broad, Mercier or interchange modes are unstable over the wide range of Δ_v and there is no second stable region, although the equilibrium beta limit increases. This fact is attributed to the small Shafranov shift.

Topologies of a single particle orbit in LHD are divided into circulating particles, toroidally trapped particles, helically trapped particles, and transition particles. Circulating particles are well confined. However, the confinement of helically trapped particles and transition particles becomes worse as the plasma beta increases, since the spectrum of the magnetic field strength becomes more complicated with increasing beta. The confinement of energetic particles has been extensively calculated and it is found that the confinement is improved with inward shift of the plasma position both in vacuum field and finite beta equilibrium. Figure 2 illustrates some typical examples of particle orbits in the LHD plasma with vanishing beta value. The particle orbits are drawn in the Boozer coordinates[16]. The torus center is on the left hand side. Trajetories of deeply trapped particles are drawn in Fig.2-(a) (mod $B_{\min}$ contours) and transition particle orbits are shown in Fig.2-(b). The two figures on the right hand side are for the case of $\Delta_v = -0.15$m and the two on the right hand side are the inward shifted case ($\Delta_v = -0.25$m). It is obvious that the confinement of a single particle is significantly improved with inward shift of the plasma. Ripple diffusions have been investigated using the DKES code [17] in the vacuum field case [18] and in the finite beta case [19]. It is shown that the ripple diffusion is greatly improved for the inward shift.

2.2 Standard configuration

The configuration which satisfies the three conditions ; (a) the plasma

beta limit of 5%, (b) no loss cone inside $\bar{a}_p/3$ in the vacuum field ($\bar{a}_p$ is the average radius of the last closed magnetic surface and $\bar{a}_p = 0.55 \sim 0.65$m in the vacuum field), and (c) possible divertor configuration, can be realized when $B = 3T$, $\gamma_c = 1.25$, $\Delta_v = -15$cm, and the toroidally averaged plasma cross-section is nearly circular. This configuration is called the "standard configuration". It should be noted that the standard configuration has not been optimized taking into account the bootstrap current. In a planar axis helical system, it is difficult to obtain an optimized configuration which simultaneously satisfies high β, good particle orbits (or reduced ripple diffusion), and the minimum bootstrap current. It is noted that, as mentioned in 2.1, it is necessary to realize a peaked pressure profile to obtain a high beta plasma.

2.3 Effect of net toroidal curent on the Mercier criterion

The bootstrap current and the current induced by the neutral beam injection (NBI) may flow in the plasma. The magnitude of beam driven current by NBI (Ohkawa current) has been estimated for the LHD plasma by Nakajima and Okamoto[20]. The bootstrap current in LHD will be discussed in the following section 2.4. Here, we investigate the effect of the net toroidal current on the Mercier criterion [10]. The profile of the net toroidal current density is assumed to be $J = J_0(1 - \Phi_n)^2$. We consider two cases for the total net toroidal current I : $I = -50$kA (subtractive case) and $I = +50$kA (additive case), and compare them with the currentless case in the standard configuration. The net toroidal current changes the poloidal magnetic field which leads to the deformation of the profile of the rotational transform. The subtractive case decreases the rotational transform and the additive case increases the rotational transform. The enhancement of the magnetic shear with increasing beta, which is favorable for the Mercier stability, is seen in the peripheral region in the subtractive case. The reduction in $\iota(0)$ in the subtractive case enhances the Shafranov shift with increasing beta value, while the shift in the additive case is smaller than that in the currentless case due to the enhancement of $\iota(0)$. The large shift of the magnetic axis in the subtractive case extends the region of the magnetic well. Thus, in the subtractive case, the self-stabilizing effects in the magnetic shear and the magnetic well is increased by the reduction of $\iota(0)$. making a stabilizing contribution to the Mercier criterion. In the standard configuration, the unstable

region is eliminated completely by the -50A net current. On the other hand, the additive current degrades the stability. Thus it is obvious that the net current affects significantly the plasma confinement in heliotron/torsatrons with magnetic shears.

2.4 Current-driven mode

The stability against the ideal current driven mode at $\beta \simeq 0\%$ are studied in the standard configuration. Calculations are carried out with the RESORM code [21] for fixed boundary equilibria. In the above range of the current (-50kA $\leq I \leq +50A$), any unstable current driven mode can not be found. As the additive current increases, the rotational transform at the magnetic axis becomes large. The internal kink mode with $m = 1$ is stable up to $I = 300$kA, although there exists $\iota = 1$ rational surface in the peripheral region. When the additive current reaches $I = 300$kA, $\iota(0)$ exceeds unity and there are two rational surfaces with $\iota = 1$. In this case, it is found that $m = 1$ internal kink mode becomes unstable. because the region inside the inner rational surface with $\iota = 1$ has the free energy source to drive the instability. The internal kink modes with $m \geq 2$ are also unstable for $I = 300$kA. The growth rates decrease with increasing m and the modes with $m \geq 6$ are stable. However, LHD has been designed so that $I = 300$kA is the maximum permissible current which the first wall withstands if a current disruption would occur.

2.5 Bootstrap current

The bootstrap current, resulting from the balance between viscosity force and friction force, depends strongly on the magnetic configuration in helical systems. In contrast to the axisymmetric tokamak, in the non-axisymmetric system, the direction of the flow to be damped by the parallel viscosities depends on the collisionality regime of the particle species [22]. This comes from the lack of symmetry. The parallel viscosities have the following expressions:

$$\begin{bmatrix} \langle \vec{B} \cdot \nabla \cdot \overleftrightarrow{\Pi}_{a1} \rangle \\ - \langle \vec{B} \cdot \nabla \cdot \overleftrightarrow{\Theta}_{a1} \rangle \end{bmatrix} = \begin{bmatrix} \mu_{a1} & \mu_{a2} \\ \mu_{a2} & \mu_{a3} \end{bmatrix} \begin{bmatrix} \langle \vec{v}_{a1} \cdot \nabla \theta_a^* \rangle \\ -\frac{2}{5P_a} \langle \vec{q}_{a1} \cdot \nabla \theta_a^* \rangle \end{bmatrix} \tag{1}$$

where $\mu_{aj}(j = 1 \sim 3)$ are the viscosity coefficients for a-species particles and θ_a^* is the newly introduced generalized angle on flux surfaces, which determines the direction of the flow to be damped. By using the Boozer coordinate system (ψ, θ, ζ) with $\psi = \Phi/2\pi$ (Φ the toroidal flux), θ the poloidal angle, and ζ the toroidal angle, θ_a^* is expressed in terms of the linear combination of the poloidal angle θ and toroidal angle ζ:

$$\theta_a^* = (I + \langle G_{BS} \rangle_a)\theta + (J - \iota \langle G_{BS} \rangle_a)\zeta \tag{2}$$

where $\langle G_{BS} \rangle_a$ is the geometric factor, which is firstly introduced in the $1/\nu$ collisionality regime by Shaing [23], and $I(J)$ is the toroidal (poloidal) current inside (outside) of a flux surface. The geometric factor $\langle G_{BS} \rangle$ in the $1/\nu$ regime depends strongly on the magnetic field structur in contrast to the axisymmetric tokamak. The viscosity in the plateau regime was calculated by Coronado and Wobig [24], the dependence of which on the field geometry is weak (or $\langle G_{BS} \rangle$ in the plateau regime is small). The bootstrap current in the plateau regime, which was obtained by Shaing et al. [25], can be generated in the opposite direction decreasing the rotational transform. The bootstrap current in the Pfirsch-Schlüter regime is very small. Thus the geometric factor $\langle G_{BS} \rangle_a$ depends on the collisionality regime of a-species particles.

The possibility to reduce the bootstrap current in a heliotron with $L = 2$ was numerically investigated by controlling axisymmetric poloidal fields [26]. It was shown that the main factor to reduce the bootstrap current is the quadrupole component of the poloidal field. The bootstrap current in the $1/\nu$ regime reduces significantly with increasing the ellipticity of the plasma cross section. The bootstrap current control was theoretically studied by Shaing et al.[27], in which the bootstrap current in the collisionless regime ($1/\nu$ regime) can be changed by controlling the external poloidal fields. Plasma currents observed during electron cyclotron heating in ATF have been identified as bootstrap currents [28]. The currents reduced with increasing ellipticity are compared with a theory. However, collisionality regimes of electrons and ions remain uncertain in this experiment and what theory was used for comparison is not written. In Ref.[27], it is claimed that the bootstrap current can be eleminated by an appropriate external coil system. However, it should be noted that, in the configuration with a large ellipticity (the plasma cross sections is vertically elongated when toroidally averaged), the confinement of energetic particles deteriorates and the plasma is unstable against inter-

change modes. As mensioned in section 2.2, it is difficult to optimize the helical system with a planar magnetic axis taking into account the MHD stability, particle orbit, and bootstrap current simultaneously.

The bootstrap current in Ref. [26] was calculated in the vacuum magnetic field. However, the bootstrap current changes the equilibrium and the equilibia (or configuration) alters the bootstrap current. Therefore, the bootstrap current and the equilibrium must be obtained consistently. Equilibrium including the bootstrap currents are calculated iteratively using the VMEC code for the LHD plasma assuming that electrons and ions belong to the same collisionality regime [29]. It has been shown in Ref.[29] that the magnitude of the bootstrap current is sensitive to the Shafranov shift in LHD. Effects of the vertical field, quadrupole field, and the pressure profile on the bootstrap current are also investigated in this paper. However. for the MHD equilibrium with the self-consistent bootstrap current, it's dependence on B_q is weaker than that estimated from the currentless equilibrium. Actually, the bootstrap current can be reduced by B_q-control by approximately factor three. (It is not mentioned in Ref.[27] whether or not the equilibria with a current and the bootstrap current were solved iteratively.)

Another important characteristics of the bootstrap current in non-axisymmetric systems which Eqs. (1) and (2) imply is that the geometric factor has different form according to the collisionality regime which reflects different characteristics of particle orbits in different collisionalities. If electrons and ions are in different collisionalities, geometric factors are different: $\langle G_{BS}\rangle_e \neq \langle G_{BS}\rangle_i$. It is noted that the geometric factor is independent of collisionality in axisymmetric tokamaks.

Here we consider the simple electron-ion plasma. The bootstrap current is given by [22]

$$\begin{aligned}
\langle BJ_{\parallel BS}\rangle &= -L_{11}^*[\langle G_{BS}\rangle_e - \langle G_{BS}\rangle_i]en_e\frac{d\phi}{d\psi} \\
&+ L_{11}^*\left[\langle G_{BS}\rangle_e\frac{dP_e}{d\psi} + \langle G_{BS}\rangle_i\frac{dP_i}{d\psi}\right] \\
&+ L_{12}^*\langle G_{BS}\rangle_e n_e\frac{dT_e}{d\psi} \\
&- \langle G_{BS}\rangle_i L_{11}^* L_{34}^* n_i\frac{dT_i}{d\psi} \qquad (3)
\end{aligned}$$

Here, L_{ij} are transport coefficients and other notations are standard. The first term on the right hand side of this equation shows clearly that there exists a new current directly proportional to the radial electric field $(-d\phi/d\psi)$ if $\langle G_{BS}\rangle_e \neq \langle G_{BS}\rangle_i$. Thus, when electrons and ions are in different collisionality regimes ($\langle G_{BS}\rangle_e \neq \langle G_{BS}\rangle_i$), the bootstrap current proportional to the radial electric field, which does not exist in axisymmetric tokamaks, exists [22, 30]. This comes from the fact that the direction of the flow damped by the parallel viscosities is dependent on the collisionality regime in the non-axisymmetric toroidal systems due to the lack of symmetry. The term proportional to the radial electric field vanishes if the three conditions of charge neutrality, momentum conservation during the collision, and axisymmetry hold.

The connection formula between each collisionality limit is constructed and the bootstrap current in LHD is estimated by solving the connection formula and the VMEC equilibrium code iteratively [31]. If $T_e = T_i(\langle G_{BS}\rangle_e = \langle G_{BS}\rangle_i)$, the bootstrap current amounts to 50 to 150 kA according to the plasma parameters in LHD. For the plasma with $T_e \gg T_i$, where electrons and ions are supposed to be in the $1/\nu$ and plateau collisionality regime, respectively, the bootstrap current is significantly reduced with increasing radial electric field. If the radial electric field is large enough , the bootstrap current becomes even negative (flowing in the opposite direction reducing the rotational transform). This can be seen in Fig.3. Based on Ref.[22], poloidal and toroidal plasma rotations in non-axisymmetric devices are formulated [32]. The present neoclassical theory for non-axisymmetric devices has been extended to the case including momentum input source due to NBI and others [33].

2.6 Ballooning mode

The ballooning mode, which is another crucial pressure-driven mode, was considered to be stable in heliotron/torsatrons because the magnetic shear is positive, as speculated by Shafranov [34]. Cooper et al. [35] found numerically unstable high$-n$ ballooning modes in the positive $\iota'(\psi)$ region in the three dimensional equilibrium, where ι and ψ denote the rotational transform and the toroidal magnetic flux. However, it is revealed by Nakajima [36, 37] that, in a currentless equilibrium with a large Shafranov shift as in heliotron/torsatrons, the high$-n$ ballooning mode can be unstable even in the

region with positive gradient of the rotational transform. This is because the local shear in the field line bending term can be reduced by the fact that the local enhancement of the poloidal field varies in the radial direction. Since the local curvature of the field lines depends on the label of the magnetic field line, α, in heliotron/torsatrons, the eigenvalue ω^2 also depends on α. In the Mercier stable region, where the pressure profile is peaked as mentioned in the section 2.1, the level surfaces of ω^2 of unstable modes, which depend strongly on α, form a spheroid in the (ψ, θ_k, α) space, where ψ and θ_k are the label of the flux surface and the radial wave number, while they form a cylinder in axisymmetric tokamaks. Such high$-n$ modes can not be related to low$-n$ modes in this case. As mentioned in section 2.1, the Mercier modes are stable for the peaked pressure profile. Accordingly, the low$-n$ ballooning modes are expected to be stable for the peaked pressure profile.

3. Control of pitch parameter

The cross sections of the helical coils of LHD are devided into three layers in which the coil current flows. The structure consists of the inner layer (I), the middle layer (M), and the outer layer (O). If the current is flowed only in the I-layer, the pitch parameter is $\gamma_c = 1.12$ and the magnetic field is $B = 1T$. If only the O-layer is used to flow the current, $\gamma_c = 1.38$ and $B = 1T$. Full operation (currents are flowed in all the layers) can generate $B = 3T$ and $\gamma_c = 1.25$. Thus, γ_c can be changed from 1.12 to 1.38.

Vacuum magnetic field, finite β equilibria. magnetic well/hill, rotational transform. Mercier criterion. and the confinement of deeply trapped particles (mod $B_{\min}$ contours) have been investigated [38]. As γ_c increases, the magnetic well region extends and the rotational transform decreases. In the case of I-layer, there is no well region and the plasma is unstable against the Mercier mode, although the equilibrium average beta limit exceeds 10%. On the other hand, in the case of O-layer, the well region (wider than in the standard configuration), the centeral rotational transform is small, thus Shafranov shift becomes large as β increases. This configuration ($\gamma_c = 1.38$ and $B = 1T$) is completely stable against the Mercier mode up to the equilibrium beta limit of 4%.

4. Helical axis configuration

The LHD has two helical coils which are independent and not linked. The current in one helical coil (I_{h1}) and the current in another helical coil (I_{h2}) are the same ($I_{h1} = I_{h2}$) under the normal condition. However, it is possible to change the ratio $R_I = I_{h1}/I_{h2}$ since the current in each helical coil can be controlled independently. A spatial axis configuration or helical axis configuration can be created by unbalancing the coil currents ($R_I \neq 100\%$), since the unbalanced currents produce $l = 1$ Fourier component in the magnetic field strength.

We start from the LHD standard configuration and decrease the current I_{h1} keeping I_{h2} constant. The ratios of currents in the poloidal field coils are fixed. However, the magnitude of the poloidal coil currents are adjusted so that the toroidally averaged magnetic axis should remain at the same position as the standard vacuum field ($R = 3.75$m, or $\Delta_v = -15$cm). The ratio R_I is scanned from 100% to 20%.

The helical excursion of the magnetic axis increases with R_I decreases, whereas the average plasma radius decreases with decreasing R_I. In the case of vacuum field, the average plasma radius is around 0.4m and the helical axis escursion is around 0.3m for $R_I = 20\%$. The rotational transform in vacuum increases and the magnetic well region extends as R_I decreases.

The remarkable effect of the unbalanced coil currents ($R_I \neq 100\%$) is to reduce the bootstrap current. This possibility was first pointed out in Ref. [27]. Figure 4 shows the integrated bootstrap currents. The ratio R_I is changed as a parameter. I_{BS} is given by

$$I_{BS}(\Phi_n) = \Phi(\bar{a}_p)\int_0^{\Phi_n} d\Phi_n \frac{\langle \vec{J}_{BS} \cdot \vec{B} \rangle}{B^2} \tag{4}$$

where Φ is the toroidal flux and Φ_n is the normalized toroidal flux ($0 \leq \Phi_n \leq 1$) and $\langle \cdot \rangle$ denotes the flux surface average. The reduction of the bootstrap current is small in the range from $R_I = 100\%$ to $R_I = 50\%$. However, the bootstrap current decreases rapidly if R_I becomes smaller than 50% and it vanishes for $R_I \simeq 40\%$. If R_I becomes smaller than 40%, the bootstrap current flows in the reversed direction decreasing the rotational transform. In this case of reversed flow, the Mercier stability improves as mentioned in section 2.3. The drastic change in the bootstrap current is attributed to the fact that the geometric factor in the low collisionality regime ($1/\nu$ regime) depends significantly on the change in the magnetic configuration due to the helical axis excursion, while the geometrical factor does not change so much

in the plateau regime. The Fourier analysis of the magnetic field strength shows that the bumpiness component as well as the $l = 1$ comoponent is needed to make such a significant change in the bootstrap current that the direction is reversed.

5. Summary

The Large Helical Divice (LHD) is a flexible apparatus for physics experiments. It has freedoms changing the axisymmetric poloidal fields, the pitch of the helical coils, and coil currents in the two helical coils. For the normal operation ($B = 3T$, $\gamma_c = 1.25$, and $I_{h1} = I_{h2}$), the configuration has been optimized by controlling the poloidal field to obtain the standard configuration. Physics characteristics have been studied for the standard configuration. One conclusion is that the peaked pressure profile is preferable to the MHD stabilities of Mercier or interchange mode and ballooning mode. Minimizing the bootstrap current has not been included in the optimization. It is not easy to reduce the bootstrap current in the planar axis helical system. However, it has been shown that there is a possibility to reduce or even reverse the current if electrons and ions are in different collisionality regimes,

The change in the pitch parameter of the two helical coils can alter the rotational transform, magnetic well region, the plasma radius, and thus the MHD properties. Helical axis configuration can be obtained if the currents in the two helical coils are unbalanced. It is possible that the helical excursion becomes comparable to the plasma radius and the bootstrap current can be drastically decreased until its direction is reversed.

The present paper has been focused on the configuration studies on LHD. One of most important issues for LHD is to create various divertor configurations to obtain the steady state plasma. The helical divertor [39], the helical island divertor [40], and the high temperature divertor operations [39, 41] are being pursued. Physics considerations for heatings, the structure and enhancement of the radial electric field, island formation, anomalous transports, and the confinement improvement are widely studied.

Acknowledgement

The author shall be grateful to the members of theory groups at the National Institute for Fusion Science for their physics considerations on LHD.

Professors A. Iiyoshi, T. Sato, M. Fujiwara, and O. Motojima are also acknowledged for encouragement.

References

[1] W VII-A Team; Proc. Plasma Physics and Controlled Nuclear Fusion Research (Berchtesgaden), IAEA, Vol.II, 1976, p.81.

[2] M. Wakatani, S. Sudo; Plasma Phys. Control. Fusion 38 (1996) 937.

[3] J.F. Lyon, B.A. Carreras, K.K. Chipley, M.J. Cole, J.H. Harris, T.C. Jernigan, R.L. Johnson, V.E. Lynch, B.E. Nelson, J.A. Rome, J. Sheffield. P.B. Thompson; Fusion Technology 10 (1986) 179.

[4] B.A. Carreras, H.R. Hicks, J.A. Holmes, V.E. Lynch, G.H. Neilson ; Nucl. Fusion 24 (1984) 1347.

[5] K. Nishimura, K. Matsuoka, M. Fujiwara. K. Yamazaki, J. Todoroki. T. Kamimura, T. Amano, H. Sanuki, S. Okamura, M. Hosokawa, H. Yamada, S. Tanahashi, S. Kubo, Y. Takita, T. Shoji, O. Kaneko, H. Iguchi. C. Takahashi ; Fusion Technology 17 (1990) 86.

[6] S. Okamura, K. Matsuoka, K. Nishimura, K. Tsumori, R. Akiyama. S. Sakakimara, H. Yamada, S. Morita, T. Morisaki. N. Nakajima, K. Tanaka. J. Xu, K. Ida, H. Iguchi, A. Lazaros, T. Ozaki. H. Arimoto, A. Ejiri. M. Fujiwara, H. Idei, O. Kaneko, K. Kawahata, T. Kawamoto, A. Komori, S. Kubo, O. Motojima, V.D. Pustovitov, C. Takahashi, K.Toi. I.Yamada; Nucl. Fusion 35 (1995) 283.

[7] A. Iiyoshi, M. Fujiwara, O. Motojima, N. Oyabu. K. Yamazaki; Fusion Technology 17 (1990) 169.

[8] V.D. Pustovitov ; Kakuyugo-Kenkyu (J. Plasma and Fus. Res.) 70 (1994) 943.

[9] K. Uo; Nucl. Fusion 13 (1973) 661.

[10] K. Ichiguchi, N. Nakajima, M. Okamoto, Y. Nakamura, M. Wakatani; Nucl. Fusion 33 (1993) 481.

[11] S.P. Hirshman, W.I. Van Rij, P. Merkel; Comput. Phys. Commun. 43 (1986) 143.

[12] A.H. Glasser, J.M. Green, J.L. Johnson; Phys. Fluids 18 (1975) 875.

[13] Y. Nakamura, K. Ichiguchi, M.Wakatani, J.L. Johnson; J. Phys. Soc. Jpn. 58 (1989) 3157.

[14] G.Y. Fu, W.A. Cooper, R. Gruber, U. Schwenn, D.V. Anderson; Phys. Fluids B4 (1992) 1401.

[15] J.H. Harris, E. Anabitarte, G.L. Bell, J.D. Bell, T.S. Bigelow, B.A. Carreras, L.A. Charlton, R.J. Colchin, E.C. Crume, N. Dominguez, J.L. Dunlap, G.R. Dyer, A.C. England, R.F. Gandy, J.C. Glowienka, J.W. Halliwell, G.R. Hanson, C. Hidalgo-Vera, D.L. Hillis, S. Hiroe, L.D. Horton, H.C. Howe, R.C. Isler, T.C. Jernigan, H. Kaneko, J.N. Leboeuf, D.K. Lee, V.E. Lynch, J.F. Lyon, M.M. Menon, R.N. Morris, M. Murakami, G.H. Neilson, V.K. Paré, D.A. Rasmussen, C.E. Thomas, T. Uckan, M.R. Wade, J.B. Wilgen, W.R. Wing; Phys. Fluids B2(6) (1990) 1347.

[16] A.H. Boozer; Phys. Fluids 23 (1980) 904.

[17] S.P. Hirshman, K.C. Shaing, W.I. Van Rij, C.O. Beasley Jr., E.C. Crume; Phys. Fluids 29 (1986) 2951.

[18] Y. Ogawa, T. Amano, N. Nakajima, K. Yamazaki, S.P. Hirshman, W.I. Van Rij, K.C. Shaing, ; Nucl. Fusion 32 (1992) 119.

[19] R. Kanno, N. Nakajima, H. Sugama, M. Okamoto, Y. Ogawa; *"Effects of finite β and radial electric fields on neoclassical transport in the Large Helical Device"*, in preparation for publication.

[20] N. Nakajima, M. Okamoto ; J. Phys. Soc. Jpn 59 (1990) 3595.

[21] K. Ichiguchi, Y. Nakamura, M. Wakatani; Nucl. Fusion 31 (1991) 2073.

[22] N. Nakajima, M. Okamoto; J. Phys. Soc. Jpn. 61 (1992) 833.

[23] K.C. Shaing, J.D. Callen; Phys. Fluids 26 (1983) 3315.

[24] M. Coronado, H. Wobig; Phys. Fluids 29 (1986) 527.

[25] K.C. Shaing, S.P.Hirshman, J.D. Callen; Phys. Fluids 29 (1986) 521.

[26] N.Nakajima, M. Okamoto, J. Todoroki, Y. Nakamura, M. Wakatani ; Nucl. Fusion 29 (1989) 605.

[27] K.C. Shaing, B.A. Carreras, N. Daminguez, V.E. Lynch, J.S. Tolliver ; Phys. Fluids B1(8) (1989) 1663.

[28] R.J. Colchin, M. Murakami, E. Anabitarte, F.S.B. Anderson, G.L. Bell, J.D. Bell, T.S. Bigelow, E.C. Crume, J.L. Dunlap, G.R. Dyer, A.C. England, P.W. Fisher, W.A. Gabbard, J.C. Glowienka, R.H. Goulding, J.W. Halliwell, G.R. Hanson, J.H. Harris, G.R. Haste, C. Hidalgo-Vera, D.L. Hillis, S. Hiroe, L.D. Horton, H.C Howe, D.P. Hutchinson, R.C. Lsler, T.C. Jernigan, M. Kwon, R.A. Langley, D.K. Lee, J.F. Lyon, J.W. Lue, C.H. Ma, M.M. Menon, R.N. Morris, P.K. Mioduszewski, G.H. Neilson, A.L. Qualls, D.A. Rasmussen, P.S. Rogers, P.L. Shaw, T.D. Shepard, J.E. Simpkins, S. Sudo, C.E. Thomas, T.Uckan, M.R. Wade, J.B. Wilgen, W.R. Wling, H. Yamada, J.J. Zielinski; Phys. Fluids B2(6) (1990) 1347.

[29] K. Watanabe, N. Nakajima, M. Okamoto, Y. Nakamura, M. Wakatani; Nucl. Fusion 32 (1992) 1499.

[30] N. Nakajima, M. Okamoto, M. Fujiwara; Kakuyugo-Kenkyu (J. Plasma and Fus. Res.) 68 (1992) 503.

[31] K. Watanabe, N. Nakajima, M. Okamoto, K. Yamazaki, Y. Nakamura, M. Wakatani; Nucl. Fusion 35 (1995) 335.

[32] N. Nakajima, M. Okamoto; J. Phys. Soc. Jpn 60 (1991) 4146.

[33] N. Nakajima, M. Okamoto; Kakuyugo-Kenkyu (J. Plasma and Fus. Res.) 68 (1992) 46.

[34] V.D. Shafranov, Phys. Fluids 26 (1983) 357.

[35] W.A. Cooper, S.P. Hirshman, D.K. Lee; Nucl. Fusion 29 (1989) 617.

[36] N. Nakajima; *"High-mode-number ballooning modes in a heliotron/torsatron system I: Local magnetic shear"*, to be published in Phys. Plasmas.

[37] N. Nakajima; *"High-mode-number ballooning modes in a heliotron/torsatron system II: Stability"*, to be published in Phys. Plasmas.

[38] K. Ichiguchi, O. Motojima, K. Yamazaki, N. Nakajima, M. Okamoto; Nucl. Fusion 36 (1996) 1145.

[39] N. Ohyabu, T. Watanabe, H.Ji, H. Akao, T. Ono, T. Kawamura, K. Yamazaki, K. Akaishi, N. Inoue, A. Komori, Y. Kubota, N. Noda, A. Sagara, H. Suzuki, O. Motojima, M. Fujiwara, A. Iiyoshi; Nucl. Fusion 34 (1994) 387.

[40] A. Komori, N. Ohyabu, T. Watanabe, H. Suzuki, A. Sagara, N. Noda, K. Akaishi, N. Inoue, Y. Kubota, O. Motojima, M. Fujiwara, A. Iiyoshi; Proc. Plasma Physics and Controlled Nuclear Fusion Research (Sevilla), IAEA, Vol.II, 1994, p.773.

[41] W.X. Wang, M. Okamoto, N. Nakajima, S. Murakami, N. Ohyabu; Nucl. Fusion 36 (1996) 1633.

FIGURE CAPTIONS

Fig.1 Stability diagram against Mercier mode and equilibrium beta limit. Δ_v is the length of the plasma axis shift in vacuum and β_0 is the central beta value. Solid line shows the Mericer criterion ($D_I = 0$) and dotted lines are contours of Mercier level surface with the interval of $\Delta D_I = 0.1$. Hatched region is in danger of destabilizing low-n ideal interchange modes.

Fig.2 Typical particle orbits in the Boozer coordinates.
Torus center is on the left side.

Fig.3 Effect of radial electric field on the bootstrap current for $T_e = 4T_i$. ϕ_0, T_e, and T_i are electric potential, electron temperature and ion temperature at the center, respectively. Profiles of the potentail and temperatures are parabolic.

Fig.4 Bootstrap current with unbalanced helical coil currents.
I_{h1} and I_{h2} are currents in each two helical coils. I_{BS} is the integrated bootstrap current given by Eq. (4).

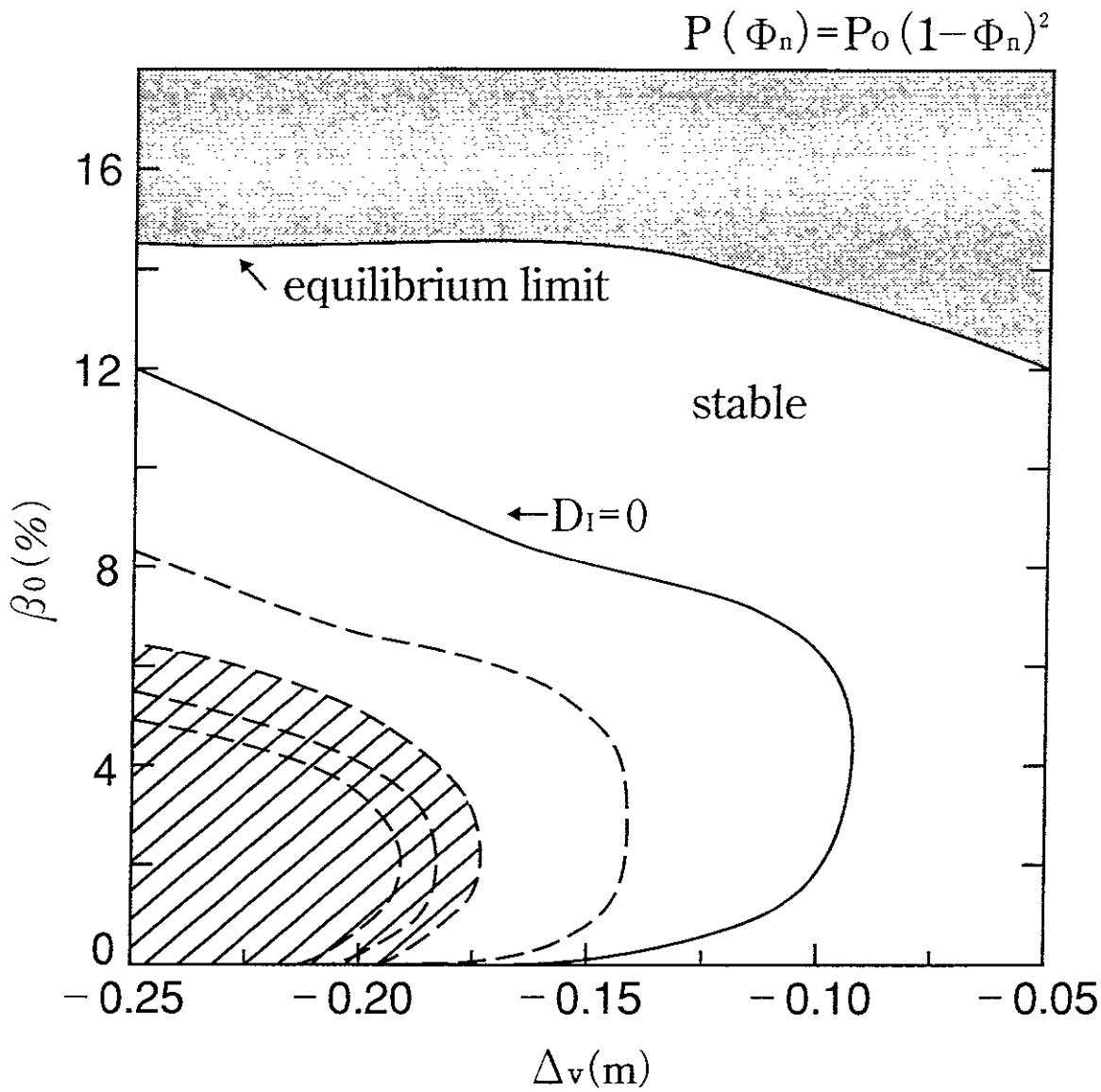
P (Φn) = P0 (1 − Φn)²
16
12
8
4
0
equilibrium limit
stable
←DI=0
β0 (%)
− 0.25
− 0.20
− 0.15
− 0.10
− 0.05
Δv(m)

Fig. 1

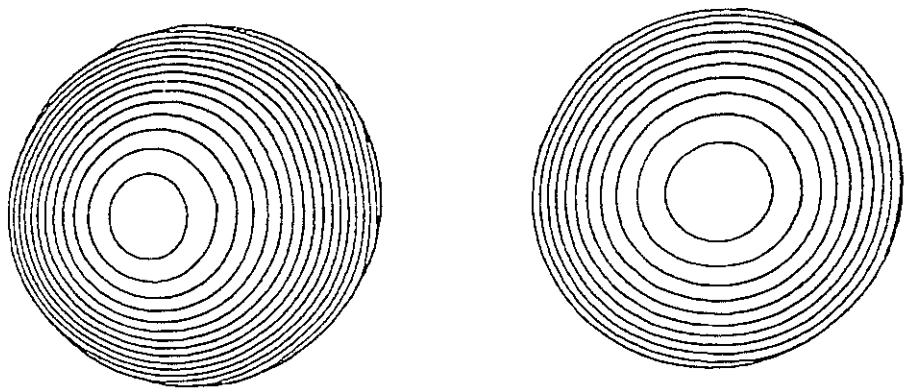

$\Delta_v = -0.15m$ $\Delta_v = -0.25m$

(a) deeply trapped particle (mod B_{min})

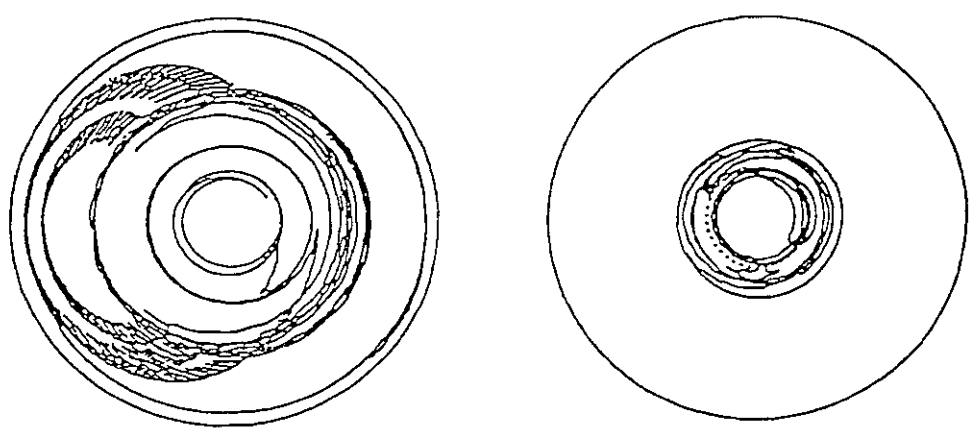

$\Delta_v = -0.15m$ $\Delta_v = -0.25m$

(b) transition particle

Fig. 2

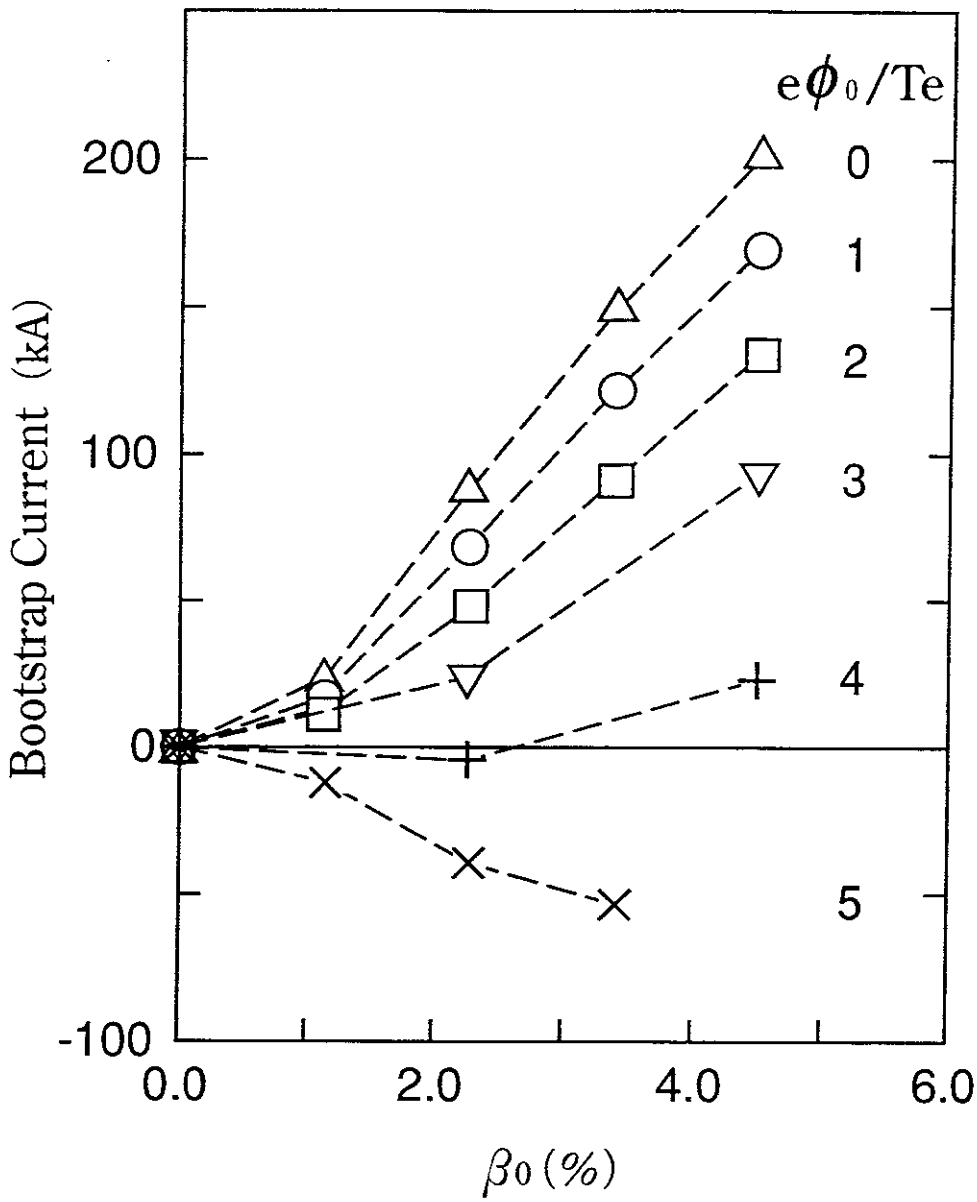

Fig. 3

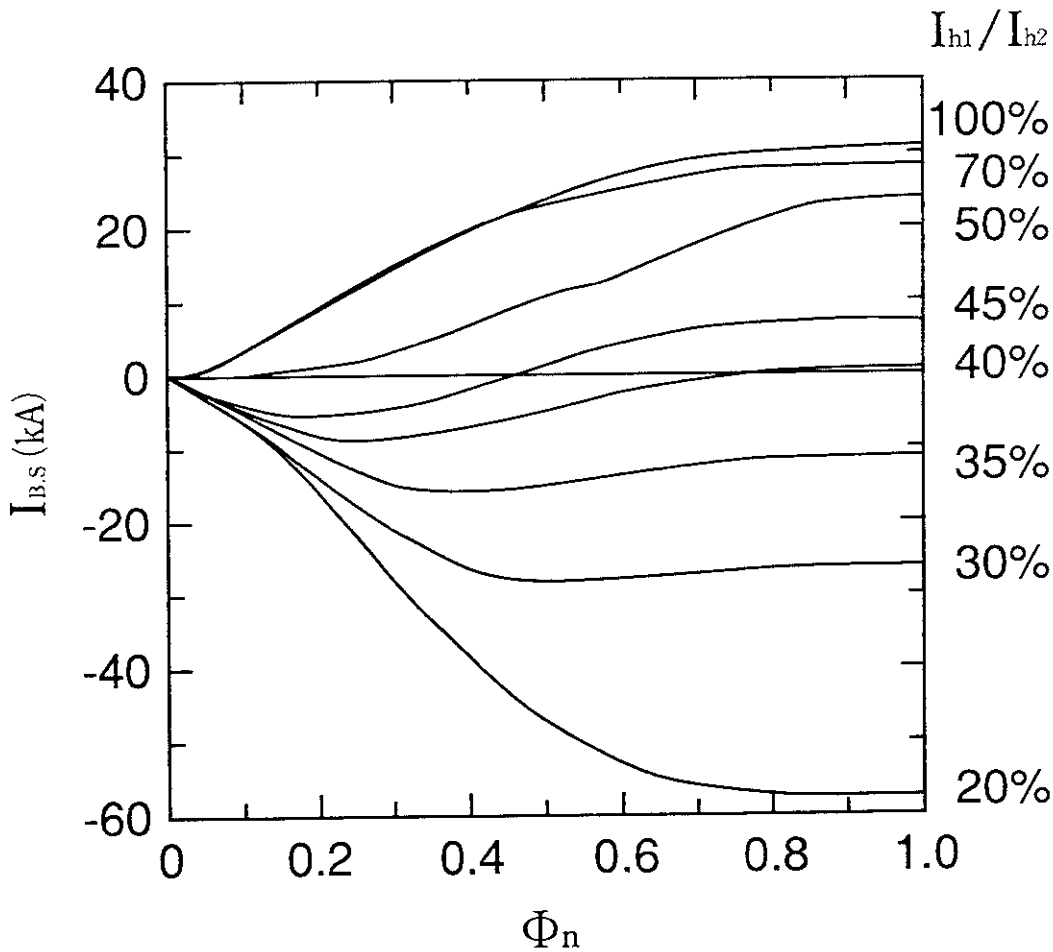
I_{h1} / I_{h2}
100%
70%
50%
45%
40%
35%
30%
20%
40
20
0
-20
-40
-60
0
0.2
0.4
0.6
0.8
1.0
$I_{B.S}$ (kA)
Φ_n

Fig. 4

Recent Issues of NIFS Series

NIFS-444 A. Fujisawa, S. Kubo, H Iguchi, H. Idei, T. Minami, H. Sanuki, K. Itoh, S. Okamura, K. Matsuoka, K. Tanaka, S. Lee, M. Kojima, T.P. Crowley, Y. Hamada, M. Iwase, H. Nagasaki, H. Suzuki, N Inoue, R. Akiyama, M. Osakabe, S. Morita, C. Takahashi, S. Muto, A. Ejiri, K. Ida, S. Nishimura, K. Narihara, I. Yamada, K. Toi, S. Ohdachi, T. Ozaki, A Komori, K. Nishimura, S. Hidekuma, K. Ohkubo, D.A. Rasmussen, J.B. Wilgen, M. Murakami, T. Watari and M. Fujiwara,
An Experimental Study of Plasma Confinement and Heating Efficiency through the Potential Profile Measurements with a Heavy Ion Beam Probe in the Compact Helical System; Sep. 1996 (IAEA-CN-64/C1-5)

NIFS-445 O. Motojima, N. Yanagi, S. Imagawa, K. Takahata, S. Yamada, A. Iwamoto, H. Chikaraishi, S. Kitagawa, R. Maekawa, S. Masuzaki, T. Mito, T. Morisaki, A. Nishimura, S. Sakakibara, S. Satoh, T. Satow, H. Tamura, S. Tanahashi. K. Watanabe, S. Yamaguchi, J. Yamamoto, M.Fujiwara and A. Iiyoshi,
Superconducting Magnet Design and Construction of LHD; Sep. 1996 (IAEA-CN-64/G2-4)

NIFS-446 S. Murakami, N. Nakajima, S. Okamura, M. Okamoto and U. Gasparino,
Orbit Effects of Energetic Particles on the Reachable β–Value and the Radial Electric Field in NBI and ECR Heated Heliotron Plasmas; Sep. 1996 (IAEA-CN-64/CP -6) Sep. 1996

NIFS-447 K. Yamazaki, A. Sagara, O. Motojima, M. Fujiwara, T. Amano, H. Chikaraishi, S. Imagawa, T. Muroga, N. Noda, N. Ohyabu, T. Satow, J.F. Wang, K.Y. Watanabe, J. Yamamoto , H. Yamanishi, A. Kohyama, H. Matsui, O. Mitarai, T. Noda, A.A. Shishkin, S. Tanaka and T. Terai
Design Assessment of Heliotron Reactor; Sep. 1996 (IAEA-CN-64/G1-5)

NIFS-448 M. Ozaki, T. Sato and the Complexity Simulation Group,
Interactions of Convecting Magnetic Loops and Arcades; Sep. 1996

NIFS-449 T. Aoki,
Interpolated Differential Operator (IDO) Scheme for Solving Partial Differential Equations; Sep. 1996

NIFS-450 D. Biskamp and T. Sato,
Partial Reconnection in the Sawtooth Collapse; Sep. 1996

NIFS-451 J. Li, X. Gong, L. Luo, F.X. Yin, N. Noda, B. Wan, W. Xu, X. Gao, F. Yin, J.G. Jiang, Z. Wu., J.Y. Zhao, M. Wu, S. Liu and Y. Han,
Effects of High Z Probe on Plasma Behavior in HT-6M Tokamak; Sep. 1996

NIFS-452 N. Nakajima, K. Ichiguchi, M. Okamoto and R.L. Dewar,
Ballooning Modes in Heliotrons/Torsatrons; Sep. 1996 (IAEA-CN-64/D3-6)

NIFS-453 A. Iiyoshi,

Overview of Helical Systems; Sep. 1996 (IAEA-CN-64/O1-7)

NIFS-454 S. Saito, Y. Nomura, K. Hirose and Y.H. Ichikawa,
Separatrix Reconnection and Periodic Orbit Annihilation in the Harper Map; Oct. 1996

NIFS-455 K. Ichiguchi, N. Nakajima and M. Okamoto,
Topics on MHD Equilibrium and Stability in Heliotron / Torsatron; Oct. 1996

NIFS-456 G. Kawahara, S. Kida, M. Tanaka and S. Yanase,
Wrap, Tilt and Stretch of Vorticity Lines around a Strong Straight Vortex Tube in a Simple Shear Flow; Oct. 1996

NIFS-457 K. Itoh, S.- I. Itoh, A. Fukuyama and M. Yagi,
Turbulent Transport and Structural Transition in Confined Plasmas; Oct. 1996

NIFS-458 A. Kageyama and T. Sato,
Generation Mechanism of a Dipole Field by a Magnetohydrodynamic Dynamo; Oct. 1996

NIFS-459 K. Araki, J. Mizushima and S. Yanase,
The Non-axisymmetric Instability of the Wide-Gap Spherical Couette Flow; Oct. 1996

NIFS-460 Y. Hamada, A. Fujisawa, H. Iguchi, A. Nishizawa and Y. Kawasumi,
A Tandem Parallel Plate Analyzer; Nov. 1996

NIFS-461 Y. Hamada, A. Nishizawa, Y. Kawasumi, A. Fujisawa, K. Narihara, K. Ida, A. Ejiri, S. Ohdachi, K. Kawahata, K. Toi, K. Sato, T. Seki, H. Iguchi, K. Adachi, S. Hidekuma, S.Hirokura, K. Iwasaki, T. Ido, M. Kojima, J. Koong, R. Kumazawa, H. Kuramoto, T. Minami, I. Nomura, H. Sakakita, M. Sasao, K.N. Sato, T. Tsuzuki, J. Xu, I. Yamada and T. Watari,
Density Fluctuation in JIPP T-IIU Tokamak Plasmas Measured by a Heavy Ion Beam Probe; Nov. 1996

NIFS-462 N. Katsuragawa, H. Hojo and A. Mase,
Simulation Study on Cross Polarization Scattering of Ultrashort-Pulse Electromagnetic Waves; Nov. 1996

NIFS-463 V. Voitsenya, V. Konovalov, O. Motojima, K. Narihara. M. Becker and B. Schunke,
Evaluations of Different Metals for Manufacturing Mirrors of Thomson Scattering System for the LHD Divertor Plasma; Nov. 1996

NIFS-464 M. Pereyaslavets, M. Sato, T. Shimozuma, Y. Takita, H. Idei, S. Kubo, K. Ohkubo and K. Hayashi,
Development and Simulation of RF Components for High Power Millimeter Wave Gyrotrons; Nov. 1996

NIFS-465 V.S. Voitsenya, S. Masuzaki, O. Motojima, N. Noda and N. Ohyabu,
On the Use of CX Atom Analyzer for Study Characteristics of Ion Component in a LHD Divertor Plasma; Dec. 1996

NIFS-466 H. Miura and S Kida,
Identification of Tubular Vortices in Complex Flows; Dec. 1996

NIFS-467 Y. Takeiri, Y. Oka, M. Osakabe, K. Tsumori, O. Kaneko, T. Takanashi, E. Asano, T. Kawamoto, R. Akiyama and T. Kuroda,
Suppression of Accelerated Electrons in a High-current Large Negative Ion Source; Dec. 1996

NIFS-468 A. Sagara, Y. Hasegawa, K. Tsuzuki, N. Inoue, H. Suzuki, T. Morisaki, N. Noda, O. Motojima, S. Okamura, K. Matsuoka, R. Akiyama, K. Ida, H. Idei, K. Iwasaki, S. Kubo, T. Minami, S. Morita, K. Narihara, T. Ozaki, K. Sato, C. Takahashi, K. Tanaka, K. Toi and I. Yamada,
Real Time Boronization Experiments in CHS and Scaling for LHD; Dec. 1996

NIFS-469 V.L. Vdovin, T.Watari and A. Fukuyama,
3D Maxwell-Vlasov Boundary Value Problem Solution in Stellarator Geometry in Ion Cyclotron Frequency Range (final report); Dec. 1996

NIFS-470 N. Nakajima, M. Yokoyama, M. Okamoto and J. Nührenberg,
Optimization of M=2 Stellarator; Dec. 1996

NIFS-471 A. Fujisawa, H. Iguchi, S. Lee and Y. Hamada,
Effects of Horizontal Injection Angle Displacements on Energy Measurements with Parallel Plate Energy Analyzer; Dec. 1996

NIFS-472 R. Kanno, N. Nakajima, H. Sugama, M. Okamoto and Y. Ogawa,
Effects of Finite-β and Radial Electric Fields on Neoclassical Transport in the Large Helical Device; Jan. 1997

NIFS-473 S. Murakami, N. Nakajima, U. Gasparino and M. Okamoto,
Simulation Study of Radial Electric Field in CHS and LHD; Jan. 1997

NIFS-474 K. Ohkubo, S. Kubo, H. Idei, M. Sato, T. Shimozuma and Y. Takita,
Coupling of Tilting Gaussian Beam with Hybrid Mode in the Corrugated Waveguide; Jan. 1997

NIFS-475 A. Fujisawa, H. Iguchi, S. Lee and Y. Hamada,
Consideration of Fluctuation in Secondary Beam Intensity of Heavy Ion Beam Prove Measurements; Jan. 1997

NIFS-476 Y. Takeiri, M. Osakabe, Y. Oka, K. Tsumori, O. Kaneko, T. Takanashi, E. Asano, T. Kawamoto, R. Akiyama and T. Kuroda,
Long-pulse Operation of a Cesium-Seeded High-Current Large Negative Ion Source; Jan. 1997

NIFS-477 H. Kuramoto, K. Toi, N. Haraki, K. Sato, J. Xu, A. Ejiri, K. Narihara, T. Seki, S. Ohdachi, K. Adati, R. Akiyama, Y. Hamada, S. Hirokura, K. Kawahata and M. Kojima,
Study of Toroidal Current Penetration during Current Ramp in JIPP T-IIU with Fast Response Zeeman Polarimeter; Jan., 1997

NIFS-478 H. Sugama and W. Horton,
Neoclassical Electron and Ion Transport in Toroidally Rotating Plasmas; Jan. 1997

NIFS-479 V.L. Vdovin and I.V. Kamenskij,
3D Electromagnetic Theory of ICRF Multi Port Multi Loop Antenna; Jan. 1997

NIFS-480 W.X. Wang, M. Okamoto, N. Nakajima, S Murakami and N. Ohyabu,
Cooling Effect of Secondary Electrons in the High Temperature Divertor Operation; Feb. 1997

NIFS-481 K. Itoh, S.-I. Itoh, H. Soltwisch and H.R. Koslowski,
Generation of Toroidal Current Sheet at Sawtooth Crash; Feb. 1997

NIFS-482 K. Ichiguchi,
Collisionality Dependence of Mercier Stability in LHD Equilibria with Bootstrap Currents; Feb. 1997

NIFS-483 S. Fujiwara and T. Sato,
Molecular Dynamics Simulations of Structural Formation of a Single Polymer Chain: Bond-orientational Order and Conformational Defects; Feb. 1997

NIFS-484 T. Ohkawa,
Reduction of Turbulence by Sheared Toroidal Flow on a Flux Surface; Feb. 1997

NIFS-485 K. Narihara, K. Toi, Y. Hamada, K. Yamauchi, K. Adachi, I. Yamada, K. N. Sato, K. Kawahata, A. Nishizawa, S. Ohdachi, K. Sato, T. Seki, T. Watari, J. Xu, A. Ejiri, S. Hirokura, K. Ida, Y. Kawasumi, M. Kojima, H. Sakakita, T. Ido, K. Kitachi, J. Koog and H. Kuramoto,
Observation of Dusts by Laser Scattering Method in theJIPPT-IIU Tokamak Mar. 1997

NIFS-486 S. Bazdenkov, T. Sato and The Complexity Simulation Group,
Topological Transformations in Isolated Straight Magnetic Flux Tube; Mar. 1997

NIFS-487 M. Okamoto,
Configuration Studies of LHD Plasmas; Mar. 1997